Distinguishing the effect of diapir growth on magnetic fabrics of syn-diapiric overburden rocks: Basque-Cantabrian basin, Northern Spain

Ruth Soto[1*], Elisabet Beamud[2,3], Eduard Roca[3], Eloi Carola[3], Ylenia Almar[4]

1 IGME. C/ Manuel Lasala, 44, 9B, 50006 Zaragoza, Spain.
2 Laboratori de Paleomagnetisme CCiTUB-ICTJA CSIC. ICT "Jaume Almera", Solé i Sabarís, s/n, 08028 Barcelona, Spain.
3 Institut GEOMODELS-Group Geodynamics and Basin Analysis, Universitat de Barcelona, 08028 Barcelona, Spain
4 ICT "Jaume Almera", CSIC, Solé i Sabarís, s/n, 08028 Barcelona, Spain

*Corresponding author. Tel.: +34 976 555 153; Fax: +34 976 553 358. *E-mail address:* r.soto@igme.es

Abstract

An analysis of Anisotropy of Magnetic Susceptibility was done on Aptian-Albian sediments from the Basque-Cantabrian basin. Thirty-nine sites were collected from the halokinetic sequences of the Bakio, Bermeo, Guernica and Mungia diapirs; 28 sites were sampled close to diapirs and 11 sites far from the diapir edges. The magnetic foliation is parallel to bedding, suggesting it reflects depositional and compaction processes, whereas the orientation of magnetic lineation varies. Far from the diapir edges, the magnetic lineation is interpreted as being related to the regional Pyrenean compression. Close to diapir edges, the observed behaviour shows that diapirs, predominantly formed by rigid ophites, have acted as buttress forming shadow areas at their northern faces protected from the Pyrenean compression. The high sensitivity of AMS allows considering it a very useful tool to distinguish deformation in halokinetic sequences related to diapir growth and/or subsequent compression.

Keywords: magnetic fabrics, salt tectonics, diapir, halokinetic sequences, Bakio diapir

Introduction

The full characterisation of strata adjacent to salt structures is fundamental in exploration and exploitation of geologic reservoirs, despite they often appear hidden in seismic lines and good outcrop examples are scarce. Deformation studies in these strata have been mostly based on the analysis of mesoscale structures from outcrop examples (e.g. Rowan et al., 1999, 2003; Giles and Rowan, 2012; Hearon et al., 2015; Poprawski et al., 2014; Alsop et al., 2015, 2016). In this work, we propose the use of the Anisotropy of Magnetic Susceptibility (AMS) to analyse the deformation of salt-related synkinematic strata. This use is important since it can give information even in absence of strain markers and/or poorly developed mesoscale brittle structures. It can be also applied to subsurface diapirs as AMS data can be reoriented to geographic coordinates using paleomagnetic data.

AMS represents a powerful tool for geologists, as it gives information related to the petrofabric of rocks. In structural studies, it represents a recognised indicator of deformation (e.g. Hrouda, 1982), even in very subtle deformed rocks which lack strain markers (e.g. Kissel et al., 1986). Applied to salt tectonics, AMS data obtained from rocks outcropping in the interior of salt structures can give information in relation to diapiric flow or internal deformation (Smíd et al., 2001; Soto et al., 2014; Santolaria et al., 2015). We have selected several diapirs, in the Basque-Cantabrian basin, which display well-exposed halokinetic sequences and suitable rocks for AMS analysis, to study the power of this approach in such geological settings.

Geological setting

The study area is located in the northern margin of the Basque-Cantabrian basin, nowadays part of the southern Eurasian plate (Fig. 1). The Basque-Cantabrian basin was developed during the Mesozoic Pyrenean rift associated with the opening of the North Atlantic Ocean and Bay of Biscay (García-Mondéjar, 1996). From the Late Cretaceous, the African plate began to drift northwards conditioning the convergence between Iberia and Europe and the inversion of the Basque-Cantabrian basin in the context of the Pyrenean orogeny (Gómez et al., 2002) (Fig. 1).

The study area is characterised by Triassic to Cenomanian rocks deformed by a large WNW-ESE fold locally pierced by several salt diapirs (Bakio, Bermeo, Guernica and Mungia diapirs) (Cuevas and Tubia, 1985) (Figs. 1 and 2). These diapirs are composed of Triassic evaporites, red clays and basic subvolcanic rocks (ophites) and flanked by Jurassic to Cretaceous materials. The ophites constitute their caprock and due to their high resistance to erosion dominate the outcrops (Fig. 2). They are flanked by Aptian-Albian syn-diapiric rocks organised in sequences limited by angular unconformities becoming conformable as distance to the diapir edges increases. These sequences are characterised by lateral facies variations and mass-transported deposits created at the diapir roofs, typical of halokinetic hooks and wedges triggered by diapir growth (Ferrer et al., 2014; Poprawski et al., 2016; Roca et al., 2016). The geometry of these halokinetic sequences was not modified during the subsequent Pyrenean compression with the exception of the NNW-SSE folds located to the South of the Bakio diapir and a slight E-W folding to the West of the Bermeo diapir (Fig. 2). The Pyrenean compression inverted the northern part of the Basque-Cantabrian basin by means of north-directed thrusts that propagated from South to North and the development of a cleavage mostly oriented E-W to ENE-WSW in the study area (e.g. Gómez et al., 2002) (for example Fig. 3, site BK01). Locally, as in site BK03, cleavage together with faults and tension gashes are associated to syn-diapiric layer-parallel slip of a thick bed of breccias with irregular base above marls occurred during syn-diapiric drape folding (Fig. 3).

Sampling and laboratory analysis

Thirty-nine sites (6 to 12 cores per site) of Aptian-Albian marls, marly limestones, fine sandstones and lutites were analysed by means of low-field AMS measured at room temperature. All sites were collected from halokinetic sequences related to the Bakio, Bermeo, Guernica and Mungia diapirs (Fig. 2). Twenty-eight sites were sampled close to diapir edges (sites located less than 1 km from the diapir walls except sites BK15 and BK59 situated between two diapirs and further from their walls, and considered related to Bermeo diapir) and 11 far from that (Table 1). The AMS analysis was done using a KLY3 from Zaragoza's University. Data were processed using Anisoft 4.2 (Chadima and Jelinek, 2009) to obtain the directional and tensor data (where K_{max}, K_{int} and K_{min} are the maximum, intermediate and minimum principal axes of the magnetic ellipsoid, respectively) and the parameters defined by Jelinek (1981), the corrected anisotropy degree Pj and the shape parameter T, ranging from -1 (prolate ellipsoid) to +1 (oblate ellipsoid).

Low-temperature AMS (LT-AMS) of 5 representative sites (6 samples per site) was measured to analyse the contributions from paramagnetic and ferromagnetic (s.l.) minerals to the total AMS and assess the significance of the low-field AMS. This was measured following the method proposed by Parés and van der Pluijm (2002). Additionally, three types of experiments were performed to characterise the ferromagnetic (s.l.) minerals: (1) thermal demagnetization of the natural remanent magnetization (NRM) of all samples using the thermal demagnetisers TSD-1

(Schonstedt) and MMTD-80 (Magnetic Measurements) and a superconducting rock magnetometer SRM 755R (2G), (2) isothermal remanent magnetisation (IRM) acquisition up to 1 T and three-axis IRM (in fields of 1.2, 0.3 and 0.1 T) thermal demagnetisation as in Lowrie (1990) using an IM10-30 pulse magnetiser (ASC Scientific), a TSD-1 thermal demagnetiser and a magnetometer JR6A (Agico), all measured in the Paleomagnetic Laboratory of Barcelona (CCiTUB-CSIC), and (3) K–T curves of selected samples using a KLY3.

Results

Magnetic properties and ferromagnetic (s.l.) mineralogy

The bulk magnetic susceptibility (Km) of the studied rocks ranges from 50 to 412 x 10^{-6} SI (Table 1). Most magnetic ellipsoids are oblate and the corrected anisotropy degree Pj is low (Pj≤1.1), typical of weakly deformed sediments. A significant correlation between Pj and lithology is observed, showing variable Pj values in a wider range between 1 and 1.1 in marls and fine sandstones, and values between 1 and 1.03 in marly limestones (Fig. 4). Km, Pj and T parameters do not show any significant variation related to distance of sites to diapir edges (Fig. 4).

K–T curves display a concave-hyperbolic shape in its initial part indicating a paramagnetic behaviour up to 300-400ºC (Fig. 5). Thermal demagnetisation of three-axis IRM shows the predominance of low coercivity minerals (< 0.1-0.3 T) and the complete demagnetisation below 590 °C in all samples (Fig. 5). Maximum unblocking temperatures of the NRM demagnetisation range between 480 and 550ºC (Fig. 5). Altogether it points to the occurrence of magnetite as the main ferromagnetic (s.l.)

phase. Although the formation of new magnetic phases upon heating obscures some of the thermomagnetic experiments, the main decrease in magnetic susceptibility below 590 °C also supports the occurrence of magnetite. Thermal demagnetisation of three-axis IRM reveals an additional and progressive IRM drop below 350 °C (Fig. 5) that might be attributed to the occurrence of either pyrrhotite and greigite (Larrasoaña et al., 2007) or maghemite (Liu et al., 2005). The increase in bulk susceptibility at low temperature with respect to its value at room temperature is similar in all samples, being the LT/RT ratio between 1.7 and 3.1 (Fig. 6), regardless of lithology or distance of sites to diapir edges. These LT/RT ratios indicate the predominance of paramagnetic minerals controlling the total AMS, which represent good markers of rock petrofabric (e.g. Oliva-Urcia et al., 2009).

Magnetic fabric

The good correspondence between axes of LT and RT-AMS magnetic ellipsoids corroborates the dominance of paramagnetic minerals to the total AMS (Fig. 7), as LT-AMS amplifies the contribution of paramagnetic minerals (Parés and van der Pluijm, 2002). Most magnetic ellipsoids show a well-defined magnetic foliation parallel to bedding with K_{min} grouped and perpendicular to bedding. The magnetic lineation, defined by K_{max}, is contained in the bedding plane in most sites (Table 1), but five sites do not have a well-defined magnetic lineation (sites BK01, BK10, BK20, BK54 and BK55; where e_{12}>45º). Site BK03 presents a prolate magnetic ellipsoid and a magnetic foliation that does not coincide neither with bedding nor cleavage (see Fig. 3) and has been discarded for further structural interpretations.

In sites located far from the diapir edges, the magnetic lineation shows a dominant WSW-ENE to E-W orientation. Close to diapir edges, however, the orientation of the magnetic lineation varies strongly depending on site location (Figs. 8 and 9). In the southeastern edge of the Bakio diapir, the magnetic lineation is oriented parallel to the diapir walls (Fig. 9); it shows a preferred NE-SW orientation in sites located in the northern sector of its eastern edge and an ENE-WSW orientation in sites located in the southern sector of the same edge. Close to the Bermeo diapir, site BK22 shows its magnetic lineation parallel to the E-W orientation of this structure and sites BK19 and BK16, BK57 and BK58, located around this diapir, show a WNW-ESE and ENE-WSW trend, respectively. Sites BK15 and BK59, considered related to Bermeo diapir and located between the Bermeo and Guernica diapirs, show a roughly N-S trend for the magnetic lineation. And the magnetic lineation orientation of site BK61 is parallel to the Guernica diapir wall (Fig. 9). A remarkable feature is that sites located at the northern edges of diapirs have magnetic lineation oriented perpendicular or highly oblique to diapir walls. These orientations are A) roughly N-S (sites BK51 and BK62 in Bakio diapir and, BK15 and BK59 in Bermeo diapir), B) NE-SW (site BK28 in Bermeo diapir) and C) NW-SE (site BK27 in Bakio diapir) contrasting with the orientation shown by sites located at thesouthern edges of the diapirs. All sites without a defined magnetic lineation (BK01, BK10, BK20, BK54 and BK55) are also located on the northern sides and close to diapirs (Fig. 9).

Discussion

The magnetic foliation of all sites, except for site BK03, is parallel to bedding and has been interpreted related to depositional and compaction processes. On the contrary, the orientation of the magnetic lineation varies through the studied area and has been interpreted as controlled by tectonic processes. Far from the diapir edges, the magnetic lineation shows a WSW-ENE to E-W trend (Fig. 8). We interpret it as related to the N-S Pyrenean compression. This interpretation is justified as a cleavage associated with the Pyrenean orogeny is observed in the studied area. Formation of cleavage and/or incipient cleavage is able to reorient a previous magnetic fabric (Soto et al., 2007; Oliva-Urcia et al., 2013). Sedimentary processes triggering the magnetic lineation acquisition can be discarded, as its orientation does not coincide neither with paleocurrents (turbidites were sourced in the North, but they were driven by the diapir relief) nor with slumping (triggered by the diapir growth) directions detected in the Bakio diapir by Poprawski et al. (2014) (Fig. 2).

Close to the diapir edges, two different types of behaviour are observed (Fig. 9). Sites located on the southern sides of diapirs show a magnetic lineation parallel to the diapir walls. We interpret the magnetic lineation observed at the southern walls associated to the Pyrenean compression stresses deviated around the diapirs. These diapirs are mainly composed of hard subvolcanic rocks (ophites) that act as a buttress hinding the northward propagation of deformation and producing stress perturbations able to reorient the magnetic lineation parallel to the diapir walls (Fig. 9). On the northern sides of diapirs, however, the magnetic lineation is either perpendicular/highly oblique to the diapir walls or could not be defined. In this case, we interpret the magnetic lineation associated to the outer-arc extension occurred during salt rise (e.g. Giles and Rowan, 2012) (see Fig. 10). Magnetic lineation in extensional scenarios coincides with the stretching direction (e.g. Mattei et al., 1997), therefore, it is expected that outer-arc extension related to salt rise also orients the magnetic lineation parallel to the extensional direction which would be perpendicular to the salt wall ridge (Fig. 10). The occurrence of sites without defined magnetic lineation and with magnetic lineation acquired during Mesozoic diapir growth points to the existence of areas ("shadow area") protected from the subsequent Cenozoic Pyrenean compression at the northern edges of the diapirs due to the presence of rigid ophites (Fig. 9). This work highlights the potential of AMS studies applied to halokinetic sequences to characterise their outer-arc deformation and so, identifying the trend of the diapir edges. It also indicates that caution is required in interpreting magnetic lineations from halokinetic sequences if subsequent tectonic events are present.

Conclusion

The application of AMS to syn-diapiric overburden rocks highlights its potential to study deformation in halokinetic sequences related to passive salt rise. Aptian-Albian turbiditic series from the Basque-Cantabrian basin have been analysed. Paramagnetic minerals dominate the total AMS validating AMS results in terms of reflecting the petrofabric of the studied rocks. The observed magnetic foliation is parallel to bedding and the orientation of the magnetic lineation variable and related to different deformation processes. Far from the diapir edges, magnetic lineation is related to the Cenozoic Pyrenean compression which propagated from South to North. Close to the diapirs, it shows the effect of diapirs filled with ophites as rigid bodies deflecting Pyrenean compression at their southern faces and protecting Mesozoic syn-diapiric deformation at their shadow areas located to the North.

Acknowledgements

Funding came from projects CGL2014-54118-C2-1-R and CGL2014-54118-C2-2-R (Spanish Ministry). Thanks to the University of Zaragoza and the Paleomagnetic

Laboratory (CCiTUB-ICTJA CSIC) where the AMSand rock-mag analyses were carried out. We are grateful to Frederic Escosa and to Mark Dekkers for his constructive comments.

References

Alsop, G.I., Weinberger, R., Levi, T., Marco, S., 2015. Deformation within an exposed salt wall: recumbent folding and extrusion of evaporites in the Dead Sea Basin. Journal of Structural Geology 70, 95-118.

Alsop, G.I., Weinberger, R., Levi, T., Marco, S., 2016. Cycles of passive versus active diapirism recorded along an exposed salt wall. Journal of Structural Geology 84, 47-67, doi: 10.1016/ j.jsg.2016.1001.1008.

Chadima, M., Jelinek, V., 2009. Anisoft 4.2, Anisotropy Data Browser for Windows. www.agico.com.

Cuevas, J., Tubia, J.M., 1985. Estructuras diapíricas asociadas al sinclinorio de Vizcaya. Munibe 37, 1-4.

EVE, 1991. Mapa geológico del País Vasco. Escala 1:25:000. Hoja 38-I (Bermeo). Ente Vasco de la Energía.

EVE, 1992. Mapa geológico del País Vasco. Escala 1:25:000. Hoja 38-III (Mungia). Ente Vasco de la Energía.

EVE, 1993a. Mapa geológico del País Vasco. Escala 1:25:000. Hoja 37-II (Arminza). Ente Vasco de la Energía.

EVE, 1993b. Mapa geológico del País Vasco. Escala 1:25:000. Hoja 37-IV (Getxo). Ente Vasco de la Energía.

Ferrer, O., Arbués, P., Roca, E., Giles, K., Rowan, M.G., De Matteis, M., Muñoz, J.A., 2014. Effect of Diapir Growth on Synkinematic Deepwater Sedimentation: The Bakio Diapir (Basque-Cantabrian Basin, Northern Spain). American Association of Petroleum Geologists Annual Convention and Exhibition, Houston, USA.

García-Mondéjar, J., 1996. Plate reconstruction of the Bay of Biscay. Geology 24(7), 635-638.

Giles, K.A., Rowan, M.G., 2012. Concepts in Halokinetic-Sequence Deformation and Stratigraphy. In: Archer, S.G., Alsop, G.I., Hartley, A.J., Grant, N.T., Hodgkinson, R. (Eds.), Salt Tectonics, Sediments and Prospectivity vol. 363. Geological Society of London, Special Publications, pp. 7–31.

Gómez, M., Vergés, J., Riaza, C., 2002. Inversion tectonics of the northern margin of the Basque Cantabrian Basin. Bull. Soc. géol. France 173, 449-459.

Hearon, T.E., Rowan, M.G., Giles, K.A., Kernen, R.A., Gannaway, C.E., Lawton, T.F., Fiduk, J.C., 2015. Allochthonous salt initiation and advance in the northern Flinders and eastern Willouran ranges, South Australia: using outcrops to test subsurface-based models from the northern Gulf of Mexico. AAPG Bulletin 99, 293–331.

Hrouda, F., 1982. Magnetic anisotropy of rocks and its application in geology and geophysics. Geophys. Surveys 5, 37-82.

Jelinek, V., 1981. Characterization of the magnetic fabrics of rocks. Tectonophysics 79, 63-67.

Kissel, C., Barrier, E., Laj, C., Lee, T.Q., 1986. Magnetic fabric in “undeformed” marine clays from compressional zones. Tectonics 5, 769-781.

Lowrie, W., 1990. Identification of ferromagnetic minerals in a rock by coercivity and unblocking temperature properties. Geophys. Res. Lett. 17, 159-162.

Larrasoaña, J.C., Roberts, A.P., Musgrave, R.J., Gràcia, E., d , Piñero, E., Vega, M., Martínez-Ruiz, F., 2007. Diagenetic formation of greigite and pyrrhotite in gas hydrate marine sedimentary systems. Earth and Planetary Science Letters 261, 350-366.

Liu, Q., Deng, C., Yu, Y., Torrent, J., Jackson, M.J., Banerjee, S.K., Zhu, R., 2005. Temperature dependence of magnetic susceptibility in an argon environment: implications for pedogenesis of Chinese loess/palaeosols. Geophysical Journal International 161, 102-112.

Lüneburg, C.M., Lampert, S.A., Lebit, H.D., Hirt, A.M., Casey, M., Lowrie, W., 1999.

Magnetic anisotropy, rock fabrics and finite strain in deformed sediments of SW Sardinia (Italy). Tectonophysics 307, 51-74.

Mattei, M., Sagnotti, L., Faccenna, C., Funicello, R., 1997. Magnetic fabric of weakly deformed clay-rich sediments in the Italian peninsula: Relationship with compressional and extensional tectonics. Tectonophysics 271, 107-122.

Oliva-Urcia, B., Larrasoaña, J.C., Pueyo, E.L., Mata, P., Parés, J.M., Schleicher, A.M., Pueyo, O., 2009. Disentangling magnetic subfabrics and their link to deformation processes in cleaved sedimentary rocks from the Internal Sierras (west central Pyrenees, Spain) Journal of Structural Geology 31, 163-176.

Oliva-Urcia, B., Román-Berdiel, T., Casas, A.M., Bógalo, M.F., Osacar, C., García-Lasanta, C., 2013. Transition from extensional to compressional magnetic fabrics in the Cretaceous Cabuérniga basin (North Spain). Journal of Structural Geology 46, 220-234.

Parés, J.M., van der Pluijm, B.A., 2002. Phyllosilicate fabric characterization by Low-Temperature Anisotropy of Magnetic Susceptibility (LT-AMS). Geophys. Res. Lett. 29(24), 2215.

Pedreira, D., Pulgar, J.A., Gallart, J., Torné, M., 2007. Three-dimensional gravity and magnetic modeling of crustal indentation and wedging in the western Pyrenees-Cantabrian Mountains. J. Geophys. Res., 112, B12405, doi:10.1029/2007JB005021.

Poprawski, Y., Basile, C., Agirrezabala, L.M., Jaillard, E., Gaudin, M., Jacquin, T., 2014. Sedimentary and structural record of the Albian growth of the Bakio salt diapir (the Basque Country, northern Spain). Basin Research 26, 746-766.

Poprawski, Y., Basile, C., Jaillard, E., Gaudin, M., Lopez, M., 2016. Halokinetic sequences in carbonate systems: An example from the Middle Albian Bakio Breccias Formation (Basque Country, Spain). Sedimentary Geology 334, 34-52.

Roca, E., Butillé, M., Ferrer, O., Arbués, P., Rowan, M.G., Giles, K.E., de Matteis, M., Muñoz, J.A., 2016. Salt tectonics and salt-sediment interaction around the Bakio diapir, Basque-Cantabrian basin, Pyrenees. AAPG/SEG International Conference & Exhibition. Barcelona, 3-6 April 2016.

Rowan, M.G., Jackson, M.P.A., Trudgill, B.D., 1999. Salt related fault families and fault welds in the northern Gulf of Mexico. AAPG Bulletin, v. 83, p. 1454–1484.

Rowan, M.G., Lawton, T.F., K.A. Giles, Ratliff, R.A., 2003. Near-salt deformation in La Popa basin, Mexico, and the northern Gulf of Mexico: A general model for passive diapirism. AAPG Bulletin 87, no. 5, 733–756.

Santolaria, P., Casas, A.M., Soto, R., 2015. Anisotropy of magnetic susceptibility as a proxy to assess internal deformation in diapirs: case study of the Naval salt wall (Southern Pyrenees). Geophys. J. Int. 202 (2), 1207-1222.

Smíd, J., Schulmann, K., Hrouda, F., 2001. Preliminary data on the AMS fabric in salt domes from the SW part of Zagros Mts., Iran. Geolines 13, 114–115.

Soto, R., Casas-Sainz, A.M., Villalaín, J.J., Oliva-Urcia, B., 2007. Mesozoic extension in the Basque–Cantabrian basin (N Spain): Contributions from AMS and brittle mesostructures. Tectonophysics 445 (3-4), 373-394.

Soto, R., Beamud, E., Oliva-Urcia, B., Roca, E., Rubinat, M., Villalaín, J.J., 2014. Applicability of magnetic fabrics in rocks associated with the emplacement of salt structures (the Bicorb–Quesa and Navarrés salt walls, Prebetics, SE Spain). Tectonophysics 629, 319–334.

Figure captions

-Figure 1. Location of the study area in the frame of the Basque-Cantabrian basin, northern Spain, and cross-section across the Basque-Cantabrian basin (modified from Pedreira et al., 2007).

-Figure 2. Geological map of the study area showing bedding plane data from field work and from EVE (1991, 1992, 1993a, 1993b), location of sites and paleocurrent directions from Poprawski et al. (2014).

-Figure 3. In situ magnetic ellipsoids of sites BK01 and BK03 showing their relationship with bedding and cleavage planes. Lower-hemisphere equal area stereoplots.

-Figure 4. Pj-T graphs in function of different lithologies indicating sites sampled close or far from the diapir edges (circle and square symbols, respectively).

-Figure 5. Representative examples of rock magnetic experiment results. (a-d) Thermomagnetic curves in argon atmosphere. Heating and cooling curves are in red and blue, respectively. Insets show enlarged heating curves. (e, f) Thermal progressive demagnetisation of the natural remanent magnetisation (NRM). (g, h, i) Three-axes IRM demagnetisation as in Lowrie (1990).

-Figure 6. Ratio between the magnetic susceptibility (Km) at low and room temperature (LT/RT) where LT/RT=3.8 corresponds to perfect paramagnetic behaviour (Lüneburg et al., 1999).

-Figure 7. Stereoplots of the RT-AMS (left), LT-AMS (middle) and T–Pj diagrams (right) differentiating the RT- and LT-AMS values for each site. Confidence ellipses for AMS principal axes are shown. Lower-hemisphere equal-area stereoplots after bedding tilt correction.

-Figure 8. Stereoplot showing K_{max} (magnetic lineation), density plot and rose diagram after bedding tilt correction for sites located far from the diapir edges and for sites located close to Bakio and Bermeo diapirs. Lower-hemisphere equal area stereoplot.

-Figure 9. Geological map of the study area showing the magnetic lineation (K_{max}) after bedding tilt correction and magnetic lineation trajectories. Magnetic lineation of sites located close to diapir edges is represented in red, whereas black lines represent magnetic lineation of sites located far from the diapir edges. Sites BK01, BK10, BK20, BK54 and BK55 do not show defined magnetic lineation and site BK03 has been discarded for further structural interpretations (see text for further explanation). Magnetic fabric acquired during or shortly after the deposition syn-diapiric rocks is only observed at the shadow areas located on the northern faces of diapirs (see text for further explanation).

-Fig. 10. Active/inactive outer-arc deformation model related to salt rise in halokinetic sequences. The main stretching direction at the active stretching area is perpendicular to the salt wall ridges. The analysis of inactive stretched areas of rocks previously placed in the arching salt wall roof reveals that magnetic lineation would be also oriented perpendicular to the salt wall ridge in protected areas (i.e. where subsequent Pyrenean compression is not able to reorient the magnetic fabric).

Table captions

-Table 1. Site means of magnetic parameters measured at room temperature.

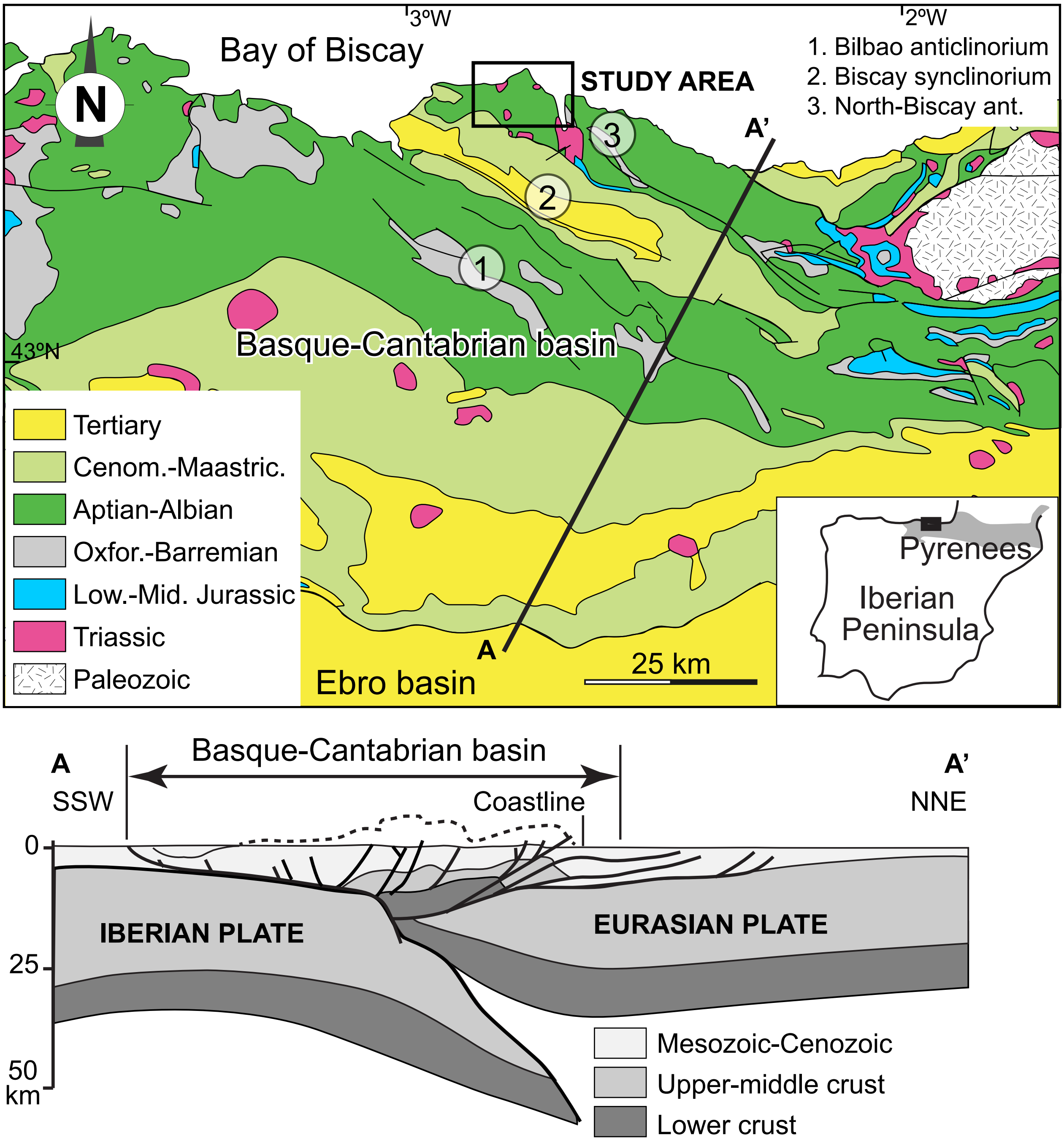
3°W
2°W
Bay of Biscay
N
STUDY AREA
1. Bilbao anticlinorium
2. Biscay synclinorium
3. North-Biscay ant.
A'
1
2
3
43°N
Basque-Cantabrian basin
Tertiary
Cenom.-Maastric.
Aptian-Albian
Oxfor.-Barremian
Low.-Mid. Jurassic
Triassic
Paleozoic
A
Ebro basin
25 km
Pyrenees
Iberian Peninsula
A
SSW
Basque-Cantabrian basin
Coastline
A'
NNE
0
25
50 km
IBERIAN PLATE
EURASIAN PLATE
Mesozoic-Cenozoic
Upper-middle crust
Lower crust

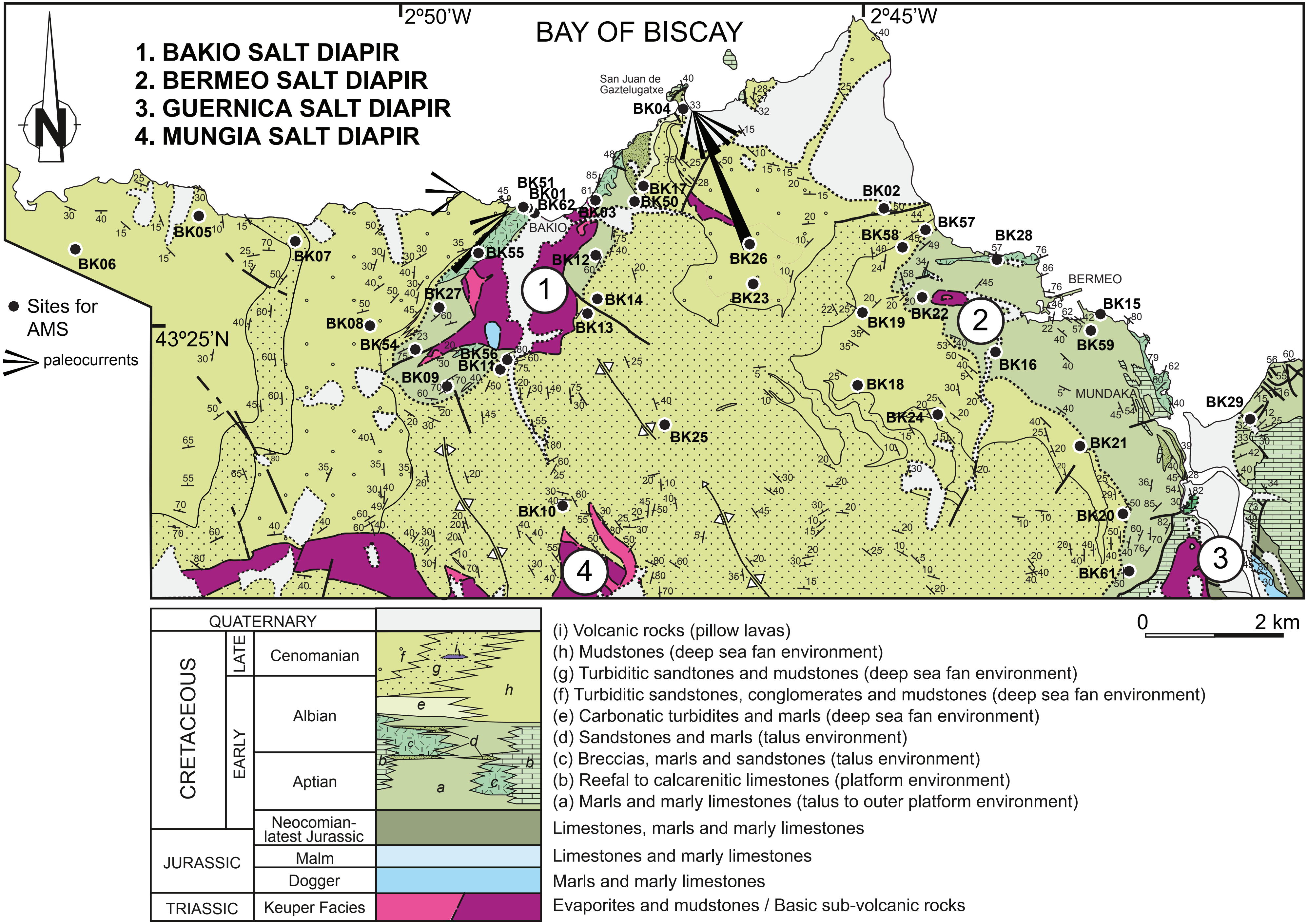

1. BAKIO SALT DIAPIR
2. BERMEO SALT DIAPIR
3. GUERNICA SALT DIAPIR
4. MUNGIA SALT DIAPIR
N
2º50'W
2º45'W
43º25'N
BAY OF BISCAY
San Juan de Gaztelugatxe
BAKIO
BERMEO
MUNDAKA
Sites for AMS
paleocurrents
BK01
BK02
BK03
BK04
BK05
BK06
BK07
BK08
BK09
BK10
BK11
BK12
BK13
BK14
BK15
BK16
BK17
BK18
BK19
BK20
BK21
BK22
BK23
BK24
BK25
BK26
BK27
BK28
BK29
BK50
BK51
BK54
BK55
BK56
BK57
BK58
BK59
BK61
BK62
0
2 km
QUATERNARY
CRETACEOUS
LATE
EARLY
Cenomanian
Albian
Aptian
Neocomian-latest Jurassic
JURASSIC
Malm
Dogger
TRIASSIC
Keuper Facies
(i) Volcanic rocks (pillow lavas)
(h) Mudstones (deep sea fan environment)
(g) Turbiditic sandtones and mudstones (deep sea fan environment)
(f) Turbiditic sandstones, conglomerates and mudstones (deep sea fan environment)
(e) Carbonatic turbidites and marls (deep sea fan environment)
(d) Sandstones and marls (talus environment)
(c) Breccias, marls and sandstones (talus environment)
(b) Reefal to calcarenitic limestones (platform environment)
(a) Marls and marly limestones (talus to outer platform environment)
Limestones, marls and marly limestones
Limestones and marly limestones
Marls and marly limestones
Evaporites and mudstones / Basic sub-volcanic rocks

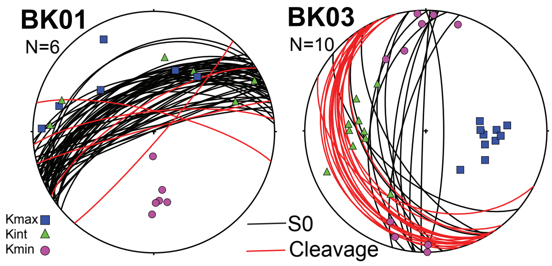

BK01
N=6
BK03
N=10
Kmax
Kint
Kmin
S0
Cleavage

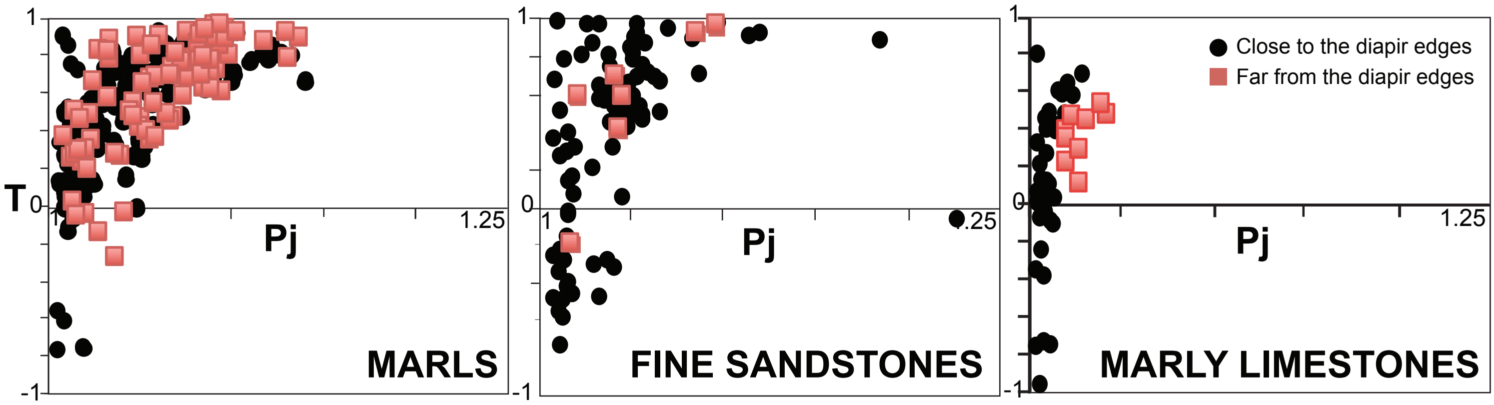
T
Pj
MARLS
FINE SANDSTONES
MARLY LIMESTONES
Close to the diapir edges
Far from the diapir edges
1
0
-1
1.25

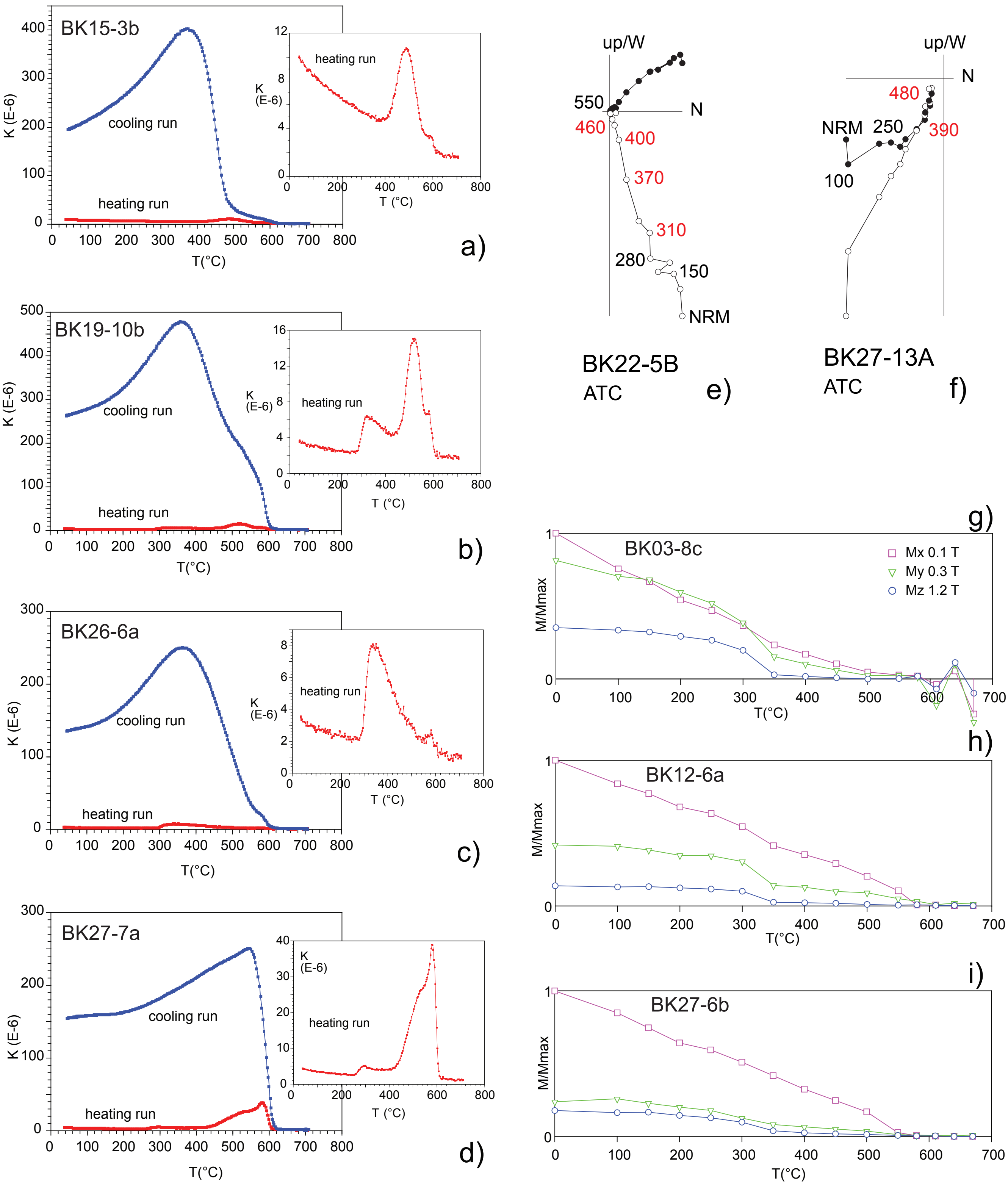

BK15-3b
K (E-6)
cooling run
heating run
T(°C)
a)
BK19-10b
b)
BK26-6a
c)
BK27-7a
d)
up/W
N
550
460
400
370
310
280
150
NRM
BK22-5B
ATC
e)
480
250
390
100
BK27-13A
f)
g)
BK03-8c
Mx 0.1 T
My 0.3 T
Mz 1.2 T
M/Mmax
h)
BK12-6a
i)
BK27-6b

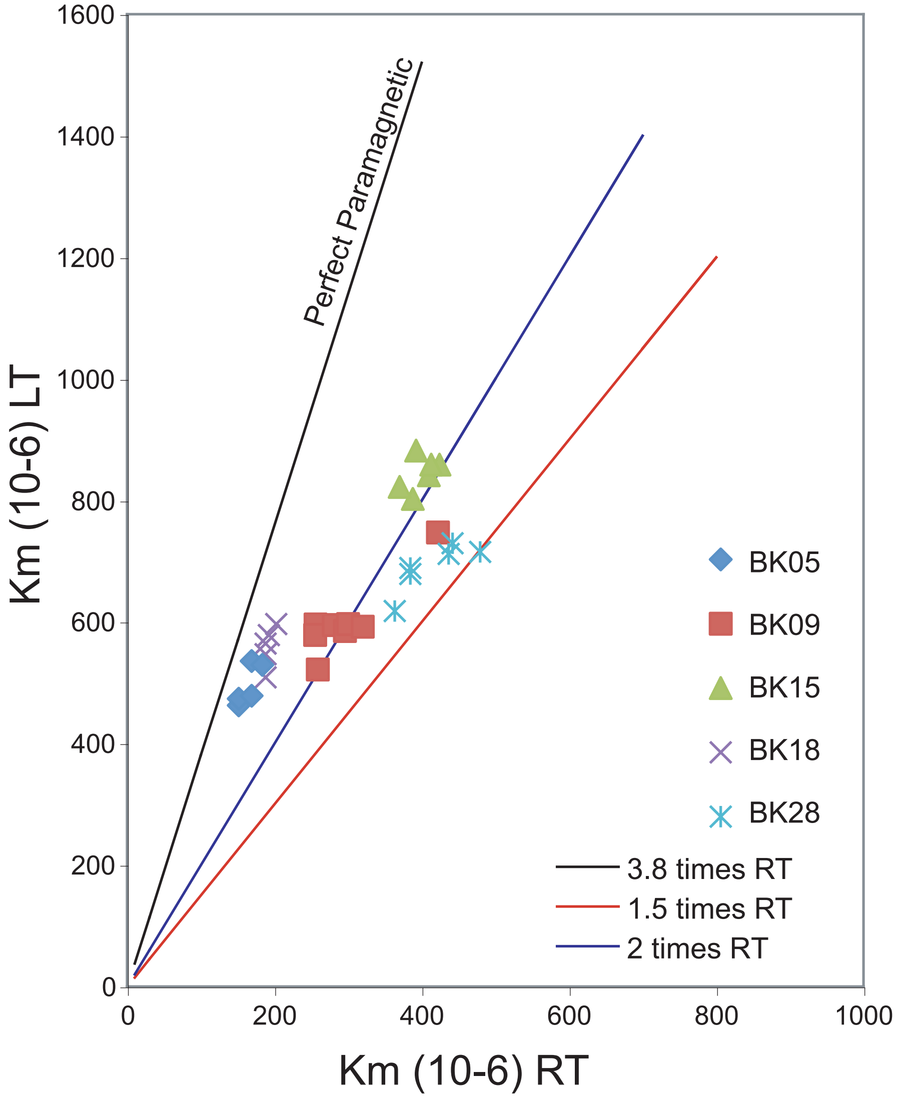

Perfect Paramagnetic
Km (10-6) LT
Km (10-6) RT
1600
1400
1200
1000
800
600
400
200
0
0
200
400
600
800
1000
BK05
BK09
BK15
BK18
BK28
3.8 times RT
1.5 times RT
2 times RT

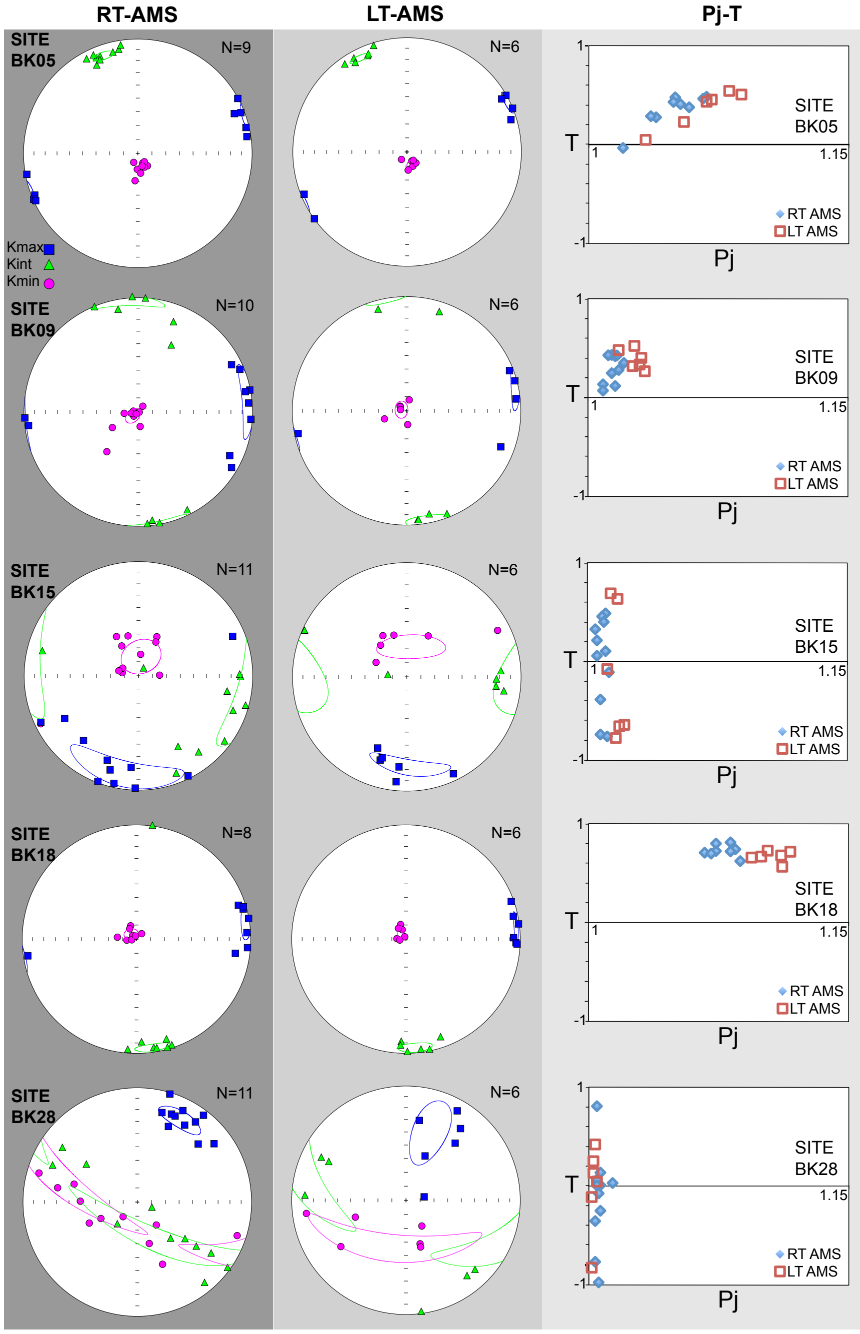
RT-AMS
LT-AMS
Pj-T
SITE BK05
N=9
N=6
Kmax
Kint
Kmin
SITE BK09
N=10
N=6
SITE BK15
N=11
N=6
SITE BK18
N=8
N=6
SITE BK28
N=11
N=6
T
Pj
1
-1
1.15
RT AMS
LT AMS

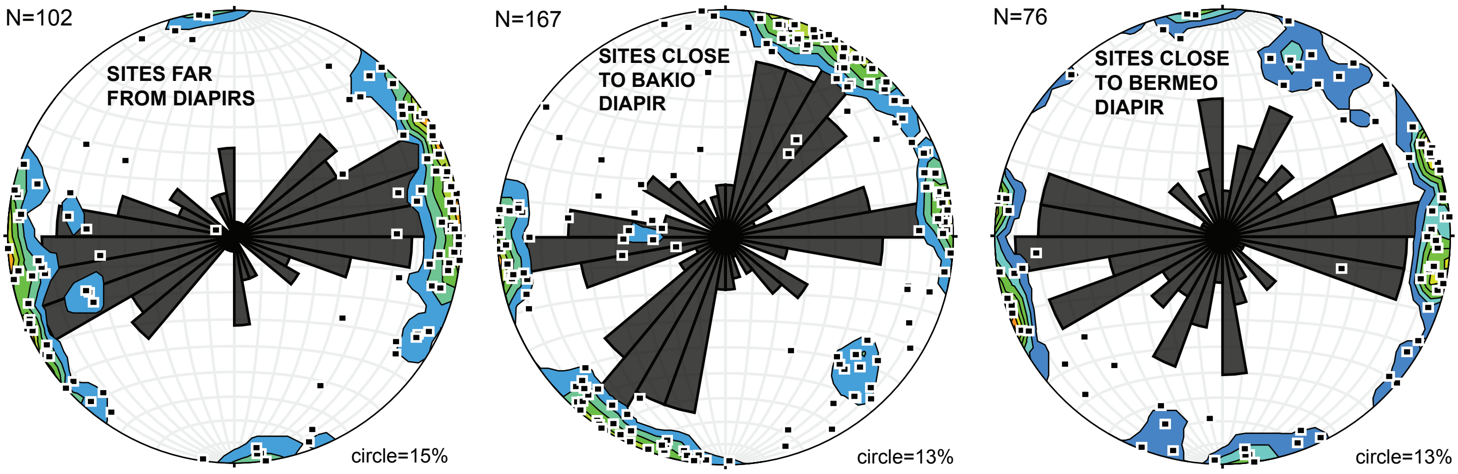
N=102
SITES FAR
FROM DIAPIRS
circle=15%
N=167
SITES CLOSE
TO BAKIO
DIAPIR
circle=13%
N=76
SITES CLOSE
TO BERMEO
DIAPIR
circle=13%

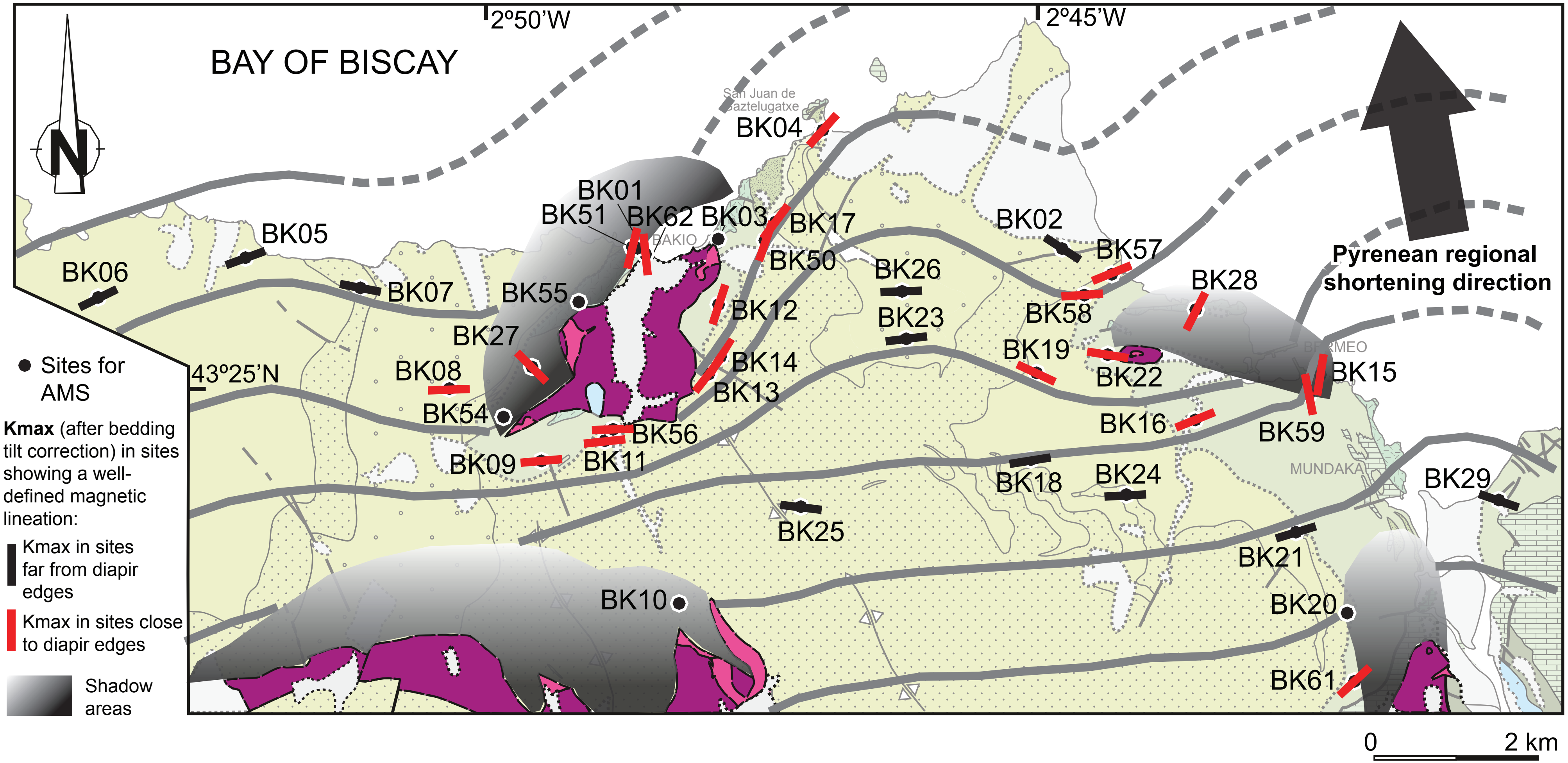

2°50'W
2°45'W
BAY OF BISCAY
N
San Juan de Gaztelugatxe
BK04
BK01
BK51
BK62
BK03
BK17
BAKIO
BK05
BK06
BK07
BK55
BK50
BK26
BK02
BK57
BK28
Pyrenean regional shortening direction
BK12
BK23
BK58
BK27
BK19
BK22
BERMEO
BK15
43°25'N
BK08
BK14
BK13
BK54
BK56
BK16
BK59
BK09
BK11
BK18
BK24
MUNDAKA
BK29
BK25
BK21
BK10
BK20
BK61
Sites for AMS
Kmax (after bedding tilt correction) in sites showing a well-defined magnetic lineation:
Kmax in sites far from diapir edges
Kmax in sites close to diapir edges
Shadow areas
0
2 km

DEFORMATION RELATED TO DIAPIR GROWTH: